Supplement of Hydrol. Earth Syst. Sci., 26, 3785–3803, 2022
https://doi.org/10.5194/hess-26-3785-2022-supplement

Hydrology and Earth System Sciences
Open Access
EGU

Supplement of

Remotely sensed reservoir water storage dynamics (1984–2015) and the influence of climate variability and management at a global scale

Jiawei Hou et al.

Correspondence to: Jiawei Hou (jiawei.hou@anu.edu.au)

$$t = R\frac{\sqrt{N-2}}{\sqrt{1-R^2}} \qquad \text{(S1)}$$

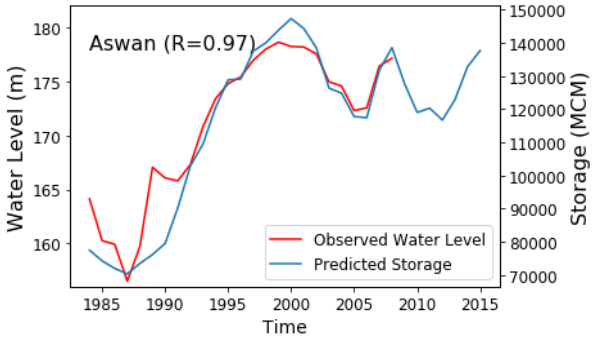

Figure S1 Validation of reservoir storage reconstruction for Lake Aswan.

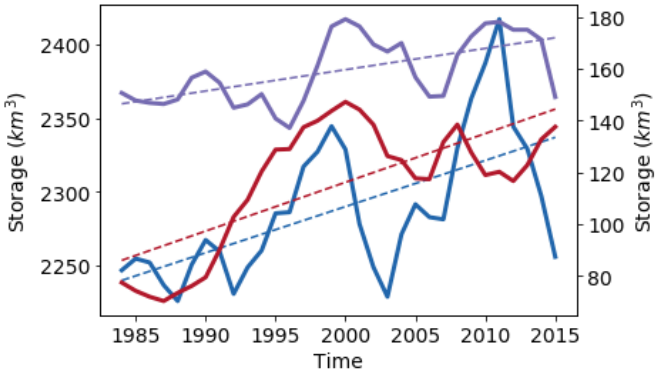

Figure S2 Annual time series (dash line: significant trends) in combined global reservoir storage (blue line; unit corresponds to left axis), and in storage for Lake Kariba (purple line; unit corresponds to right axis), and Lake Aswan (red line; unit corresponds to right axis).

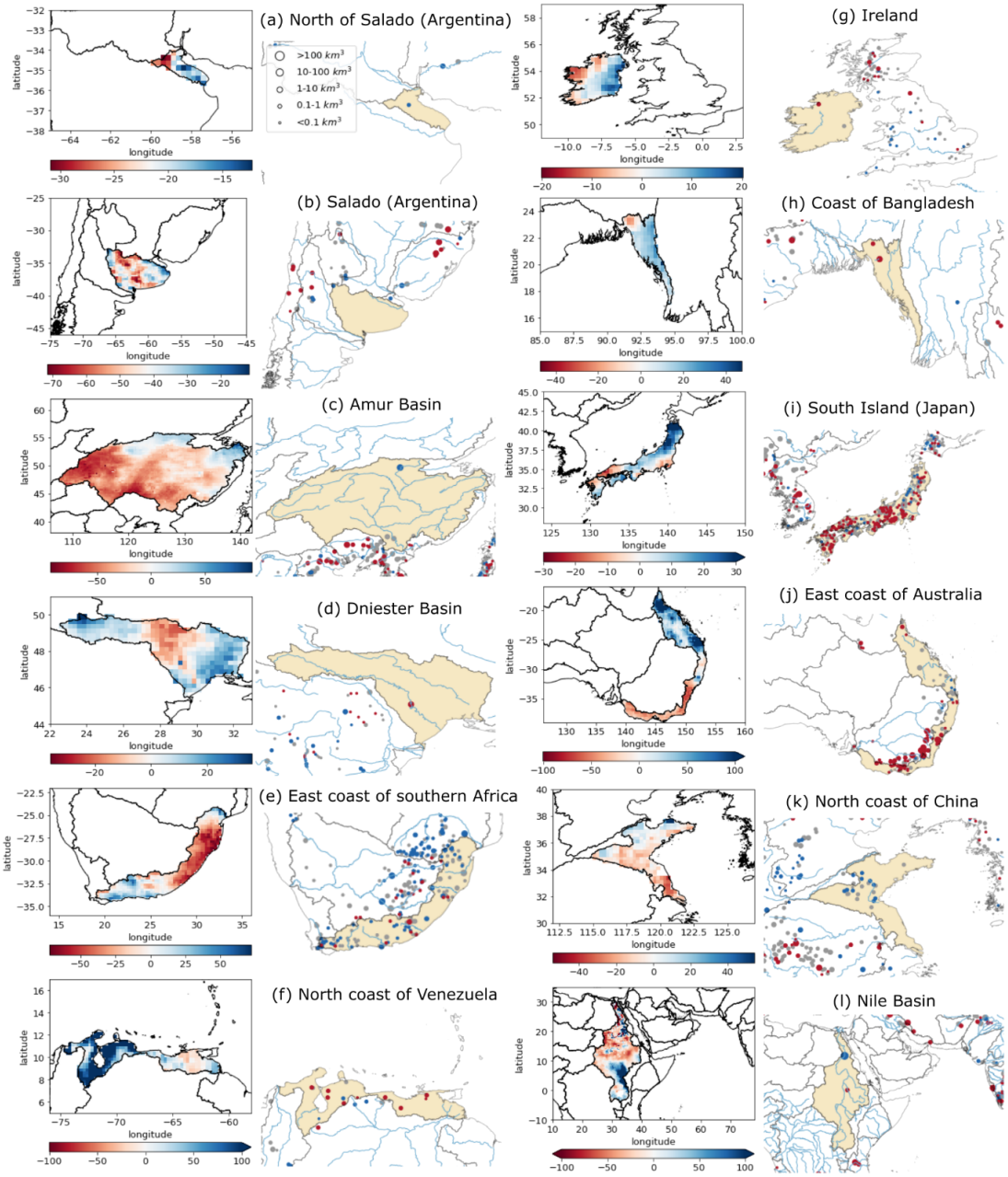

Figure S3 Trends in reservoir storage (second and fourth column; $p<0.05$; increasing: blue; no change: grey; decreasing: red; dot sizes correspond to storage capacity; light blue line: main river network; faded yellow shade: selected basins) and grid-based modelled streamflow (first and third column; colour correspond to per cent of linear change overall period) during 1984–2015.

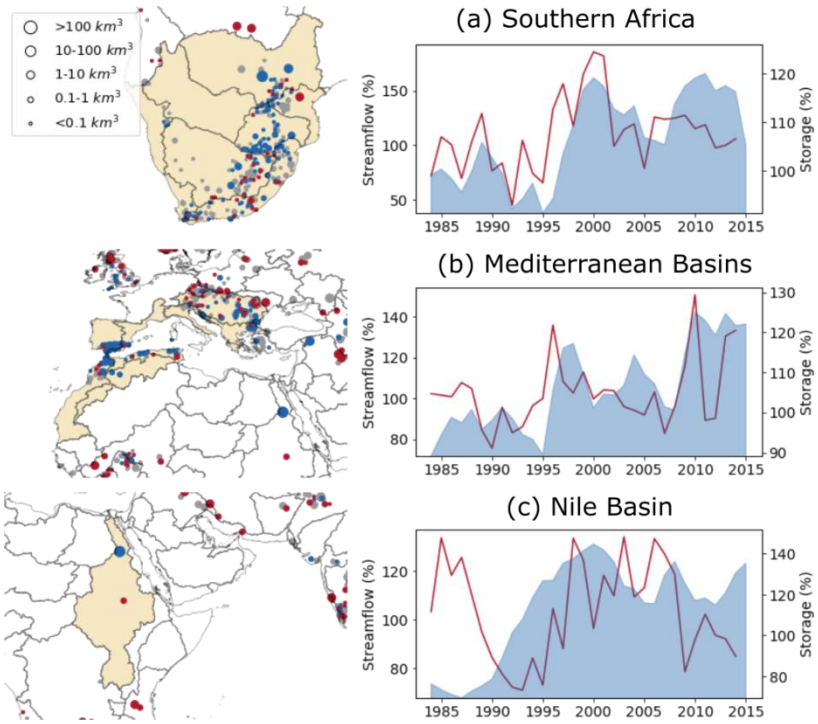

Figure S4 Trends in reservoir storage (first column; p<0.05; increasing: blue; no change: grey; decreasing: red; dot sizes correspond to storage capacity; faded yellow shade: selected regions) and time series of annual average relative total storage volume (light blue shaded), and modelled streamflow (solid red line) indicated with a base period of 1984–1999 (second column).

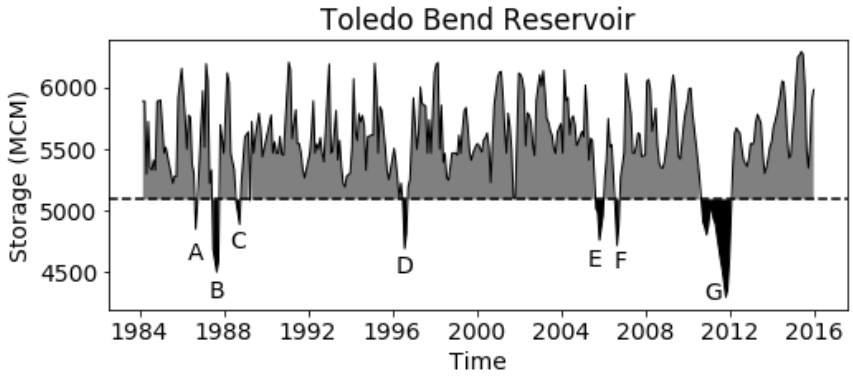

Figure S5 Example storage time series showing the definition of resilience and vulnerability (black shaded: unsatisfactory state; grey shaded: satisfactory state, dashed line: 10% threshold; letters: labelled failure events).

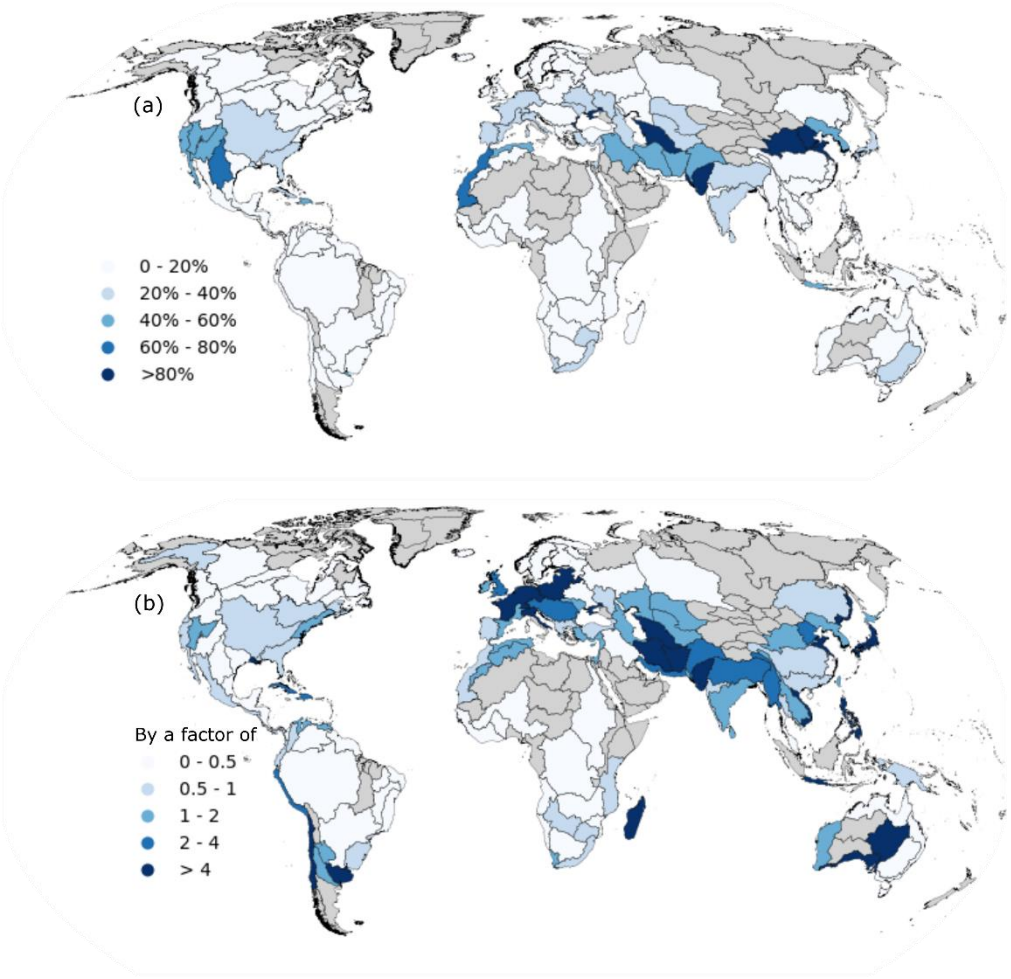

Figure S6 The ratio of the average annual total water withdrawal and total river inflow (a) and total water withdrawal and total reservoir capacity (b) in each basin. Annual withdrawal is a small or modest fraction of annual inflow in a majority of basins and water withdrawal is probably mainly from non-storage sources (i.e. groundwater, direct river extraction and reuse) in some basins such as in central Eurasia.

Table S1 The list of original sources of gauging data (listed in ascending order of number of stations)

National and international sources	The number of gauging data
The United States Geological Survey (USGS) National Water Information System (NWIS: https://waterdata.usgs.gov/nwis) and GAGES-II database (Falcone (2011))	9180
The Global Runoff Data Centre (GRDC: http://grdc.bafg.de; Lehner (2012))	4628
The HidroWeb portal of the Brazilian Agência Nacional de Águas (http://www.snirh.gov.br/hidroweb)	3029
The European Water Archive (EWA) of EURO-FRIEND-Water (http://ne-friend.bafg.de)	2260
Water Survey of Canada (WSC) National Water Data Archive (HYDAT; https://www.canada.ca/en/environment-climate-change)	1479
The National Center for Atmospheric Research (Dai, 2016)	925
The Australian Bureau of Meteorology (BoM: http://www.bom.gov.au/waterdata; Zhang et al. (2013))	776
The Chilean Center for Climate and Resilience Research (CR2: http://www.cr2.cl/recursos-y-publicaciones/bases-de-datos/datos-de-caudales)	531

Table S2 Statistical models to estimate reservoir depth (D: average depth; A: observed extent; S_{100}: average slope around the reservoir).

Reservoir size class by maximum extent (km^2)	Statistical models
0.1-1	$\log_{10}(D) = 0.3826 + 0.1512 \times \log_{10}(A) + 0.4820 \times \log_{10}(S_{100})$
1-10	$\log_{10}(D) = 0.1801 + 0.2985 \times \log_{10}(A) + 0.8473 \times \log_{10}(S_{100})$
10-100	$\log_{10}(D) = 0.0379 + 0.2445 \times \log_{10}(A) + 1.1517 \times \log_{10}(S_{100})$
100-500	$\log_{10}(D) = 0.0123 + 0.2664 \times \log_{10}(A) + 1.1474 \times \log_{10}(S_{100})$

Table S3 The average performance of lake volume estimation using either good quality Landsat images or gap-filling images (original ones with different contamination percentages).

Contamination Percentages	<5%	5% - 35%	35% -65%	65% - 95%
R	0.86	0.87	0.80	0.80
	0.86		0.87	

Table S4 The statistics of resilience and vulnerability for the reservoir in Fig. S5.

Period	1984-2000				2000-2015		
Failure Event	A	B	C	D	E	F	G
Duration Time (month)	2	4	3	3	5	3	18
Resilience (1/month)	0.33				0.12		
Deficit Volume (GL)	239	589	202	399	329	373	792
Vulnerability (average deficit volume)	357				498		

References:

Dai, A., Oki, Q. T. T. (Ed.): Historical and future changes in streamflow and continental runoff: a review. In: Tang Q, Oki T (eds), Chapter 2 of Terrestrial water cycle and climate change: natural and human-induced impacts, Geophysical Monograph, American Geophysical Union, 17-37 pp., 10.1002/9781118971772.ch2 2016.

Falcone, J. A.: GAGES-II: Geospatial attributes of gages for evaluating streamflow, US Geological Survey, 2011.

Lehner, B.: Derivation of watershed boundaries for GRDC gauging stations based on the HydroSHEDS drainage network. Report 41 in the GRDC Report Series. https://www.bafg.de/GRDC/EN/02_srvcs/24_rprtsrs/report_41.pdf?__blob=publicationFile, 2012.

Zhang, Y., Viney, N., Frost, A., Oke, A., Brooks, M., Chen, Y., and Campbell, N.: Collation of Australian modeller's streamflow dataset for 780 unregulated Australian catchments, Water for a Healthy Country National Research Flagship. https://publications.csiro.au/rpr/download?pid=csiro:EP113194&dsid=DS4, 2013.